NASA TECHNICAL MEMORANDUM 100600

SURFACE CRACK ANALYSIS APPLIED TO IMPACT DAMAGE IN A THICK GRAPHITE/EPOXY COMPOSITE

C. C. Poe, Jr., C. E. Harris, and D. H. Morris

APRIL 1988

NASA
National Aeronautics and Space Administration

Langley Research Center
Hampton, Virginia 23665

INTRODUCTION

Light-weight composite cases were developed for the solid rocket motors of the Space Shuttle. The cases are made of graphite/epoxy using a wet filament-winding process, hence the name filament-wound cases (FWC). Each 3.66-m-diameter (12-ft) motor consists of four cases -- a forward case, two center cases, and an aft case -- that are joined to short steel rings with pins. The forward and center cases are approximately 7.62 m (25 ft) in length, and the aft case is somewhat shorter. The FWC's are 3.6-cm (1.4-in.) thick except very near the ends where they are thicker to withstand the concentrated pin loads.

Tests [1-4] revealed that impacts by dropped objects such as tools and equipment can reduce the uniaxial tension strength of the FWC laminate, sometimes without even making a visible crater. The damage was localized to a region directly beneath the impact site and extended only partway through the laminate. The damaged region contained broken fibers, and the locus of breaks in each layer resembled a crack perpendicular to the direction of the fibers. Impacts usually cause thin composite laminates to delaminate over a relatively large region. However, the thick FWC did not delaminate, making the damage difficult to detect except with special ultrasonic techniques [5-8].

In the present paper, the impact damage in the FWC laminate is represented as an equivalent surface crack, and the residual strengths are predicted using a surface crack analysis. The stress intensity factor for a semi-elliptical surface crack in a homogeneous, isotropic plate is used for the composite plate. The value of fracture toughness was predicted using a general fracture toughness parameter for composite materials. The size of the damage or equivalent surface crack was predicted with the analysis of reference [9]. The analysis uses a maximum shear stress criterion and stresses calculated with Love's solution for pressure applied on part of the boundary of a semi-infinite body. The pressure was calculated using Hertz's law. The predicted strengths are compared with experimental values.

Original measurements were made in English units and converted to SI units.

SYMBOLS

a	depth of surface crack or impact damage, m (in.)
c	half-length of surface crack or impact damage, m (in.)
E	Young's modulus, Pa (psi)
E_{xr}	Young's modulus of remaining ligament in hoop direction, Pa (psi)
f_w	functional in equation (7)
f_ϕ	functional in equation (7)

$F(a/t,a/c,c/W,\phi)$	functional in equations (4), (5), and (7)
g	functional in equation (7)
G	shear modulus, Pa (psi)
K	stress intensity factor, $Pa\sqrt{m}$ ($psi\sqrt{in.}$)
K_Q	fracture toughness, $Pa\sqrt{m}$ ($psi\sqrt{in.}$)
M_1,M_2,M_3	functionals in equation (7)
n_o	factor in the Hertz law, Pa (psi)
p	contact pressure distribution, Pa (psi)
p_c	average contact pressure, Pa (psi)
P	peak impact force, N (lbf)
Q	shape factor for an elliptical crack
r_c	contact radius, m (in.)
R_i	radius of indenter, m (in.)
S_{cl}	gross stress for failure of first ligament, Pa (psi)
S_{cr}	gross stress for failure of remaining ligament, Pa (psi)
t	laminate thickness, m (in.)
W	width of specimen in test section, m (in.)
z_o	depth from surface where damage initiates
ϵ_{tu}	ultimate tensile failing strain of the undamaged laminate
ζ	ratio of damage depth to contact radius, a/r_c
ζ_o	ratio of depth to contact radius where damage initiates, z_o/r_c
ν	Poisson's ratio
τ_u	shear strength, Pa (psi)

ϕ	parametric angle of ellipse ($\phi = 0^0$ and 90^0 correspond to where the surface crack intersects the free surface and to the location of the maximum depth, respectively.)

Subscripts:

1,2	principal coordinates of the layers (The 1-direction is the fiber direction.)
x,y	Cartesian coordinates (The x-direction is the hoop direction of the FWC laminate.)
r,θ,z	cylindrical coordinates (The z-direction is normal to the plane of the laminate.)

MATERIAL

For the impact investigations [1-4], a 0.76-m-diameter (30-in.), 2.13-m-long (7-ft) full-thickness cylinder was made to represent the region of a FWC away from the ends. The cylinder was wound by Hercules Inc. using a wet process and AS4W-12K graphite fiber and HBRF-55A epoxy resin except for the hoop layers, which were hand laid using prepreg tape. The properties of the materials used in making the cylinder and the elastic constants of the laminate are given in Appendix A. From outside to inside, the orientations of the layers were $\{(\pm 33.5^0)_2/90^0/[(\underline{\pm 33.5^0})_2/90^0]_3/[(\pm 33.5^0)_2/90^0]_7/(\pm 33.5^0/90^0_2)_4/(\pm 33.5^0)_2/\text{cloth}\}$, where the 90^0 layers are the hoops and the $\pm 33.5^0$ layers are the helicals. (The layer angles are measured from the axis of the cylinder.) The underlined $\underline{\pm 33.5^0}$ helical layers are about 1.6 times as thick as the other helical layers. The cloth layer at the inner surface has an equal number of fibers in the warp and weave directions. The layup is balanced (equal numbers of $+33.5^0$ and -33.5^0 layers) but not symmetrical about the midplane. Most of the hoop layers are closer to the inner surface than the outer surface.

None of the specimens from the rings were left for the deply investigation in reference [9]. Consequently, a 30- by 30-mm (12- by 12-in.) plate that had been cut from an actual FWC was used. Because the cylinder was made to represent the FWC, the materials of the plate and cylinder were basically the same. Of course all of the layers of the plate were wound with AS4W-12K graphite fiber and HBRF-55A epoxy, and the radius of curvature of the plates was 1.8 m (6 ft). The layer orientations were also slightly different because the plate came from a FWC with an earlier design. From outside to inside, the layup of the plate was $\{(\pm 33.5^0)_2/90^0/[(\underline{\pm 33.5^0})_2/90^0]_3/[(\pm 33.5^0)_2/90^0]_7/(\pm 33.5^0/90^0_2)_2/\pm 33.5^0/90^0_4/\pm 33.5^0/90^0_2/(\pm 33.5^0)_2/\text{cloth}\}$. The FWC plate has two more hoop layers than the rings, but the outer 55 layers are the same. These differences should not affect the results in reference [9].

TEST APPARATUS AND PROCEDURE

The experiments to measure the effect of impact damage on the residual strength of the FWC are described in detail elsewhere [1-4]. Nevertheless, the apparatus and procedure are briefly described here for the convenience of the reader.

Impact Tests

The cylinder was cut into 30.5-cm-long (12-in.) rings. Two of the rings were impacted by free-falling masses. See figure 1. Inert propellant was cast in one of the rings, but the other ring was left empty. During impacts, the rings lay on a thin rubber sheet in a shallow aluminum cradle. The empty ring was secured to the concrete floor with bolts and a cross-bar to prevent the ring from "leaping" off the floor. Each ring was impacted every 5.1 cm (2.0 in.) of circumference, giving 44 impact sites. The damage did not overlap.

The free-falling impacters consisted of a 5-cm-diameter (2-in.) steel rod with a 2.54-cm-diameter (1.00-in.) indenter on the end. Four rods of different lengths were used to give masses of 2.8, 5.0, 9.0, and 18.6 kg (6.1, 11.1, 19.9, and 41.1 lbm), including the indenter. The impacter was instrumented to determine the maximum impact force. Drop heights were varied from 38 to 305 cm (15 to 120 in.) to give kinetic energies from 38 to 446 J (28 to 329 ft-lbf).

Hertz law [10] was used to calculate contact pressures from the impact forces. The pressure between a hemispherical indenter of radius R_i and a semi-infinite, transversely isotropic body is given by

$$p = \frac{3}{2} p_c \left(1 - \frac{r^2}{r_c^2}\right)^{1/2} \tag{1}$$

where r is the radius measured from the center of the contact site, r_c is the contact radius, and p_c is the average pressure given by

$$p_c = \frac{P}{\pi r_c^2} \tag{2}$$

where P is the peak or maximum impact force and

$$r_c = \left(\frac{PR_i}{n_0}\right)^{1/3} \tag{3}$$

The value of n_0 can be calculated [10] from the elastic constants of the composite. However, because the transverse Young's modulus of the FWC laminate was not accurately known, n_0 was determined experimentally [9] to be 4.52 GPa (656 ksi).

Residual Strength Tests

After the two rings were impacted, each one was cut into 44 specimens that were 30.5-cm (12-in.) long and 5.1-cm (2.0 in.) wide. Circular arcs were ground into the specimens' edges to reduce the width in the test section to 3.3 or 3.8 cm (1.3 or 1.5 in.). See figure 2. The specimens were uniaxially loaded to failure in tension with a 445-kN-capacity (100 kips) hydraulic testing machine. Stroke was programed to increase linearly and slowly with time. Hydraulically actuated grips that simulate fixed-end conditions were used. Otherwise, uniaxial loading would cause bending because the FWC laminate is not symmetrical. Bending does not develop in the pressurized motor case.

Deply Tests

The experiments in reference [9] were conducted to measure the extent of impact damage by a destructive deply technique. The impacts to the rings could not be directly reproduced with the FWC plate because the stiffness and mass of the plate and rings were different. Thus, the impacts were simulated by statically loading the plate normal to its surface with the indenter. The plate was continuously supported on the opposite surface, and the indenter was applied at the center of each of 36 test squares, where the sides of each square were 3.8 cm (1.5 in.) long. Indenters with diameters of 1.27 and 5.08 cm (0.50 and 2.00 in.) were used in addition to that with a diameter of 2.54 cm (1.00 in.). Contact pressures were calculated from the forces using equations (2) and (3). The square specimens were cut from the plate, and the layers were separated using pyrolysis. Damage in contiguous specimens did not overlap. For such a thick laminate, it is believed that the damage (as well as the value of n_0) is the same for a simulated impact and an actual impact of low velocity.

RESULTS AND ANALYSIS

This section is divided into two subsections. In the first subsection, the actual impact damage and analysis to predict the size of the damage is described. This analysis is only summarized here; a more detailed description with experimental verification is given in reference [9]. In the second subsection, strengths predicted with the surface crack analysis are presented for both semi-elliptical surface cuts and impact damage. The surface cut experiments were originally presented in reference [12] but are summarized here to verify the surface crack analysis and to show how very shallow surface cracks and impact damage were treated.

Equivalent Surface Crack for Impact Damage

Damage size measurements.- Radiographs and through-transmission ultrasonic C-scans [5-8] gave no evidence that the impacts caused delaminations. All damage was localized to a region directly beneath the impact site. An example of the type of fiber damage caused by the simulated impacts [9] is shown in figure 3. The peak applied force was 66.7 kN (15.0 kips). Photographs of the eight outermost layers of fibers are shown. (There were 76 layers in the

laminate.) The contact area is approximately at the center of the first layer. An indentation was readily visible on the surface of the specimen before pyrolysis. Broken fibers are visible in the center of the first seven layers; layers 8 and below were not damaged. The locus of breaks in each layer resembles a crack, sometimes several closely spaced cracks (barely visible in layer 4). The crack in each layer is basically perpendicular to the direction of the fibers in that layer. Thus, the cracks are not coplanar and do not make a single surface crack. Sometimes the cracks have a jog, such as in layer 7.

Photomicrographs of a highly magnified crack caused by an actual impact [2-4] are shown in figure 4. The crack was in layer 7; layers 8 and below were not damaged. This specimen was impacted with a 2.54-cm-diameter (1.00-in.) indenter, producing a contact force of 54.3 kN (12.2 kips). The photograph in figure 4(a) shows the entire crack, and the photograph in figure 4(b) shows a small portion of the crack at an even higher magnification. The fiber breaks caused by the impact resemble those caused by the simulated impact in figure 3.

Damage size predictions.- For ad hoc assessments of impact damage, it would be sufficient to determine the size with some nondestructive method. However, in order to do sensitivity studies and to design for damage tolerance requirements, an analytical capability to predict damage size is necessary. Such a capability was demonstrated in reference [9] for simulated impacts to an FWC plate using a maximum shear stress criterion for failure. The maximum shear stress was calculated using Love's solution for a semi-infinite body with pressure on part of the boundary [11]. The pressure distribution is that given by equation (1). The body is assumed to be homogeneous and isotropic. Some discrepancy is expected between this solution and that for a layered anisotropic plate like a composite. Damage contours from this analysis are plotted in figure 5 using a Poisson's ratio of 0.3 for the FWC laminate. The distance from the surface and from the center of contact are normalized by the contact radius r_c. The contours are shown for various ratios of the average contact pressure p_c to the shear strength τ_u. Damage initiates below the surface at a distance of 0.482 when the average contact pressure is $2.15\ \tau_u$. As the pressure increases, the contour increases radially in size until it reaches the surface for $p_c/\tau_u \approx 5$. The contours are somewhat elliptical in cross section initially, but become more semi-elliptical as they approach the surface. Thus, the damage region resembles an ellipsoid or "truncated" ellipsoid.

Crack lengths from two of the 20 deply tests in reference [9] are plotted against depth in figure 6 for simulated impacts. The average contact pressures were 648 and 742 MPa (94.0 and 108 ksi). The corresponding forces were 66.7 and 99.6 kN (15.0 and 22.4 kips), respectively. Note that the crack lengths are not projected onto a single plane. See the sketch in figure 6(a). The cracks were measured only on the outer side of a layer. In drawing the graph, crack length was assumed to be constant across a layer. The graph shows that the depth and length of the cracks increase with increasing contact pressure. Similar results were obtained for other pressures and indenter diameters.

Damage profiles predicted with the maximum shear stress failure criterion are also plotted in figure 6. A value of $\tau_u = 276$ MPa (40 ksi), which gave a good fit to damage depth for these two deply tests, was used to calculate the

maximum shear stress with Love's equations. The maximum length of the cracks in figure 6 is somewhat larger than predicted. For the damage contours in figure 5, the ratio of half-length to depth c/a is approximately 0.8, where values for the 20 deply tests were typically between 0.8 and 1.4. The predicted damage profile circumscribes the crack lengths fairly well except near the surface, where no damage is predicted. The damage is predicted to initiate at a depth of $0.482r_c$ and grow toward the surface as pressure is increased. In the deply tests, on the other hand, damage was always found to extend from the first layer down. The damage in the outer layers was probably caused by large inplane compressive stresses σ_r and σ_θ that diminish rapidly with distance from the surface. The state of stress near the surface is somewhat hydrostatic, causing the maximum shear stress to be relatively small. Away from the surface, σ_r and σ_θ are small and $\tau_{max} \approx 0.5\sigma_z$, much like the compression test of the disks.

For the 20 deply tests, values of damage depth predicted with τ_u = 228 and 310 MPa (33 and 45 ksi) gave upper and lower bounds. The tests included three indenter diameters and six values of average contact pressure. Compression tests were conducted on disks taken from the FWC plate, where the load was applied normal to the plane of the laminate. The average compression strength was 621 MPa (90 ksi), which corresponds to a maximum shear stress of 310 MPa (45 ksi). Thus, the analysis of the simulated impacts and the compression tests are in fair agreement. The discrepancy could be caused by the assumption of homogeneity and isotropy in Love's solution.

In predicting residual strength, the impact damage was represented as a surface crack oriented normal to the applied load. The depth and length of the crack was taken as those of the damaged region predicted with the maximum shear stress criterion. Thus, the outline of the crack approximately matches the cross section of the damaged region. See figure 7. It may seem inappropriate at first to assume that the impact damage is equivalent to a surface crack when the cracks in the helical layers do not lie in the plane of the surface crack. However, the stiffness of the helical layers and the stress in the helical layers normal to the surface of the equivalent crack are small compared to the hoop layers. Thus, the helical layers are relatively stress free and ineffective in carrying load across the crack, much as if they were cracked.

The maximum depth of the damage contours in figure 5 is given by

$$\frac{4\tau_u}{3p_c} = \left(\frac{5}{2} - \nu_t\right)(1 + \zeta^2)^{-1} + (1 - \nu_t)\zeta^2(1 + \zeta^2)^{-1} + (1 + \nu_t)\zeta \mathrm{Tan}^{-1}\left(\frac{1}{\zeta}\right) \qquad (4)$$

where $\zeta = a/r_c$. The depth $\zeta_0 = z_0/r_c$ where damage initiates is given by

$$0 = 3\zeta_0 - (1 + \nu_t)(1 + \zeta_0^2)\left[(1 + \zeta_0^2)\mathrm{Tan}^{-1}\left(\frac{1}{\zeta_0}\right) - \zeta_0\right] \qquad (5)$$

which corresponds to the location of τ_{max}. The depth of the damaged region or equivalent surface crack was calculated with equation (4), and the contact

pressure p_c was calculated from the impact force with equations (2) and (3) and $n_0 = 4.52$ GPa (656 ksi). A value of $\tau_u = 228$ MPa (33 ksi) was assumed because it best represents the minimum contact pressure for damage initiation as well as an upper bound for the damage depth. For convenience, it was assumed that the impact damage has a constant aspect ratio of $c/a = 1.0$. As noted previously, the experimental values of c/a had considerable variation.

Strength Predictions

Except for very shallow surface cuts or impact damage, the composite laminates failed in two stages: first, the cut or damaged layers broke and delaminated from the undamaged layers; and then, with additional load, the undamaged layers broke. See figure 8. The two stages of failure are referred to as first- and remaining-ligament failure. For shallow damage, the laminate failed catastrophically in one stage. Specimens with semi-elliptic surface cuts failed similarly [12]. For quasi-isotropic T300/5208 plates containing surface cuts with $c/a = 3.8$, radiographs [13] did reveal delaminations at the maximum depth or bottom of the surface cut prior to failure of the first ligament, but not for specimens with $c/a < 3.8$. Radiographs of the FWC specimens were not made prior to failure of the first ligament. But, for specimens with impact damage and surface cuts, there was no visual evidence nor did load-displacement measurements indicate that delaminations were present prior to when the first ligament failed.

Surface crack analysis for first-ligament failure.- Failure of the first ligament was assumed to occur when the maximum stress intensity factor along the front of the equivalent surface crack exceeded the fracture toughness K_Q. For an isotropic, homogeneous material, the stress intensity factor is given [14] by

$$K = S\left(\frac{\pi a}{Q}\right)^{1/2} F(a/t, a/c, c/W, \phi) \tag{6}$$

where S is the remote stress, a is the crack depth, $2c$ is the crack length, t is the plate thickness, W is the plate width, Q is the shape factor, and ϕ is the elliptical angle that specifies the location on the crack border. Where the surface cut intersects the free surface, $\phi = 0^o$ and, where the depth of the surface cut is a maximum, $\phi = 90^o$. The equations for Q and $F(a/t, a/c, c/W, \phi)$ are given in Appendix B. Replacing K by K_Q in equation (6) yields the following equation for the failing stress of the first ligament.

$$S_{c1} = \frac{K_Q}{\left(\frac{\pi a}{Q}\right)^{1/2} F(a/t, a/c, c/W, \phi)} \tag{7}$$

No fracture tests with through-the-thickness cuts were conducted to determine K_Q for the FWC laminate. Instead, a value of $K_Q = 0.949$ GPa$\sqrt{\text{mm}}$ (27.3 ksi$\sqrt{\text{in.}}$) was predicted with a general fracture toughness parameter [1-3,15].

Maximum strain criterion for remaining-ligament strength.- The hoop strain was assumed to be uniform over the remaining ligament, and failure was assumed to be governed by failure of the hoop layers. Thus, the failing strain of the remaining ligament ϵ_{tu} is independent of remaining-ligament thickness and is equal to the failing strain of the hoop fibers. Accordingly, the gross stress at failure S_{cr} is given by

$$S_{cr} = (1 - \frac{a}{t})E_{xr}\epsilon_{tu} \tag{8}$$

where E_{xr} is Young's modulus of the remaining ligament in the loading or hoop direction. Values of E_{xr}, which vary with remaining-ligament thickness, were calculated [1-4] with lamination theory. A value of $\epsilon_{tu} = 0.0124$ was derived from unnotched tensile data.

Strengths with surface cuts.- The investigation in reference [12] was conducted first to study the failure modes of the FWC laminate with part-through cuts and to determine how well strengths could be predicted using equations (7) and (8). The specimens that contained the surface cuts were taken from one of the other FWC-like rings that was not impacted. The stress for first- and remaining-ligament failures are plotted against cut depth in figures 9(a)-9(d) for $c/a = 0.5$, 1.0, 2.0, and 5.7. The stresses were divided by an undamaged strength of 379 MPa (55.0 ksi). The plane of the surface cuts was normal to the hoop direction, and the specimens were loaded in the hoop direction. The location and width of the hoop layers are shown on the abscissa to aid in interpreting the results. In most cases, each symbol represents an average of two values. Circular symbols represent 2.5-cm-wide (1.0-in.) specimens, and square symbols represent 5.1-cm-wide (2.0-in.) specimens. The widest specimens were required for the deepest cuts. The open symbols represent first-ligament failure, and the solid symbols represent remaining-ligament failures. For shallow cuts, the first failures were catastrophic and no remaining-ligament strengths are shown. For some of the deeper cuts, remaining-ligament strengths are not shown because the specimens were not reloaded after the first ligament failed. Instead, they were saved for other purposes.

The lines in figures 9(a)-9(d) represent predictions with equations (5) and (6). For first-ligament failure, the dashed lines represent 2.5-cm-wide (1.0-in.) specimens, and the solid lines represent 5.1-cm-wide (2.0-in.) specimens. Except for shallow cuts and $c/a = 2.0$ with $W = 2.5$ cm (1.0 in.), the test and predicted values of first-ligament strength are in good agreement. For shallow cuts, the predicted strengths are too large. However, the lines that are drawn tangent to the surface crack equation represent the test values quite well. Notice that the tangent lines were not drawn through the undamaged strength at $a = 0$, but through $a = 1.7$ mm (0.067 in.), which corresponds to the outer surface of the first hoop layer. It was assumed that cuts more shallow than the outer hoop layer would not reduce the strength since the outer helical layers contribute very little to the stiffness of the laminate. These lines correct the surface crack analysis for shallow cracks and are very convenient to construct. For $c/a = 5.7$, no tangent line is shown because it virtually coincides with the surface crack equation. Notice in figure 9(c) for $c/a = 2.0$ that the values of first-ligament strength for $W = 2.5$ cm (1.0 in.) and the

deepest crack are significantly less than the predicted value. These test values seem inconsistent with those for W = 5.1 cm (2.0).

The predicted curve for the remaining ligament in figures 9(a)-9(d) has a stair-stepped shape because the stiffnesses of the hoop and helical layers are very different. The large drops in stress correspond to removal of the stiff hoop layers, and the small drops correspond to removal of the more flexible helical layers. The curve is convex in the overall sense because most of the hoop layers are closer to the bottom of the laminate. The predictions of remaining-ligament strengths are 5 to 10 percent larger than the test values. After the first ligament fails, the load path in the specimens is eccentric. Although the grips are very stiff, they may allow enough bending to cause the test values to be less than the predictions.

Harris and Morris [13] had equal success in using the surface crack analysis to predict the strength of a 1.0-cm-thick (0.40-in.) T300/5208 graphite/epoxy composite containing semi-elliptical surface cuts. Strengths of specimens with through-the-thickness cuts were also predicted accurately [16]. The same value of fracture toughness, which was also predicted with a general fracture toughness parameter, was used for the surface cuts and the through-the-thickness cuts.

Recently, Wu and Erdogan [17] and Chatterjee [18] calculated the stress intensity factor for an orthotropic homogeneous plate with a semi-elliptical surface crack using a line-spring model and a finite element model, respectively. In both cases, the isotropic and orthotropic results differ significantly. The agreement between the experiments and isotropic analysis and the discrepancy between the isotropic and anisotropic analyses cannot be resolved at this time. In any event, the experiments validate the use of the isotropic surface crack equations to predict strengths.

Strengths with impact damage.- The measured and predicted stresses for first- and remaining-ligament failures are plotted against impact force in figures 10(a) and 10(b), respectively. The stresses were divided by an undamaged strength of 345 MPa (50.1 ksi). The top axis, which is not linear, gives the depth of the damage that is associated with the predictions. Circular symbols were used for the ring filled with inert propellant and square symbols for the empty ring. The specimens had widths of 3.3 and 3.8 cm (1.3 and 1.5 in.). Differences between predictions for the two widths can hardly be discerned. Thus, no distinction is made between predictions for the two widths. Two predicted curves are shown for the first-ligament failures in figure 10(a): one for the surface crack analysis given by equation (5) and one for tangent lines like those shown in figures 9(a)-9(c). The difference between the tangent line and the surface crack analysis line is significant for the smaller impact forces and damage depths. Damage is predicted to initiate at an impact force of 28.6 kN (6.43 kips) and at a depth of 2.1 mm (0.082 in.), which is below the outer hoop layer. The damage remains relatively shallow, even for the largest impact forces. The tangent line agrees with the strengths quite well. The predicted and measured remaining-ligament strengths in figure 10(b) also agree well. The remaining-ligament strengths are significantly larger than the first-ligament strengths for the larger impact forces. Thus, the thick composite laminate affords some degree of damage tolerance not given by conventional metals.

Vertical lines are drawn in figures 10(a) and 10(b) to indicate that impact forces below 75.2 kN (16.9 kips) caused only slight surface indentations that were barely visible. At this threshold, hoop stresses required to fail the first ligament were less than 80 percent of the undamaged strength. This impact force corresponds to an average contact pressure of 640 MPa (93 ksi). Recall that a pressure between 408 and 514 MPa (59.2 and 74.6 ksi) was required to initiate fiber damage. Sharper indenters [1] caused more visible surface damage, but the reductions in strength were not much more than those in figures 10(a) and 10(b). The analysis used here is capable of predicting the effect of indenter shape on residual strength and contact pressures. Therefore, the analysis can be used for preliminary design and for parametric studies to determine worst conditions and the best materials.

In figures 10(a) and 10(b), strengths for the empty ring were about 10 percent below those for the filled ring. The propellant increased the effective mass of the ring by more than a factor of seven, causing the impact forces for the filled ring to be considerably larger than those for the empty ring. Because the FWC laminate is very thick, the impact damage should be equal in the filled and empty rings for the same impact force. Thus, the difference in strengths between the filled and empty rings cannot be explained by the presence of the inert propellant.

CONCLUSIONS

A surface crack analysis was used to predict the residual strength of a thick graphite/epoxy composite after low-velocity impact. The specimens were impacted with a rod that had a 2.54-cm-diameter (1.00-in.) hemispherical indenter mounted on one end. The impacters were dropped from various heights to give various amounts of damage. The damage was localized to a region directly beneath the impact site. It extended only partway through the laminate. The damaged region contained broken fibers, and the locus of breaks in each layer resembled a crack perpendicular to the direction of the fibers. No delaminations were detected. The specimens were uniaxially loaded to failure in tension. They failed in two stages: first the damaged layers (first ligament) and then, with increasing load, the remaining undamaged layers (remaining ligament). When the damaged layers failed, they delaminated from the undamaged layers. An analysis was developed to predict the size of damage using Hertz's contact law and the maximum shear stress calculated with Love's solution for pressure applied to part of a semi-infinite body. The analysis was verified by deplying specimens and measuring the size of the impact damage. The damage was represented as a surface crack with the same width and depth. The stress to fail the first ligament was predicted with a surface crack analysis. The stress to fail the remaining ligament was predicted using a maximum strain failure criterion. The measured and predicted stresses to fail the first ligament of the impacted specimens were in good agreement. The failing stresses of the remaining ligament were a little below the predicted values, perhaps due to bending that was not taken into account.

The analysis, which takes into account the radius of the impacter and the mechanical properties of the composite, can be used for preliminary design and for parametric studies to determine worst conditions and the best materials.

APPENDIX A - MATERIAL PROPERTIES

The graphite fiber is Hercules Inc.'s AS4W-12K, and the winding resin is Hercules Inc.'s HBRF-55A. The epoxy in the unidirectional broadgoods is Hercules Inc.'s MX-16. Fiber-lot-acceptance tests were conducted on the fiber used to make the test case. Properties of the helical fiber, broadgoods fiber, and matrix or winding resin are given in Table I. (The helical and broadgoods fibers were from different lots.)

Physical properties and lamina constants were measured by Hercules Inc. on six coupons cut from the ends of the test case. The physical properties are given in Table II and the lamina constants are are given in Table III.

The elastic constants of the test case laminate were predicted with lamination theory using the lamina constants in the table above. It was assumed that bending and stretching were not coupled, that is, the laminate was symmetric. The predictions are E_x = 30.6 GPa (4.44 Msi), E_y = 39.0 GPa (5.66 Msi), G_{xy} = 19.7 GPa (2.86 Msi), ν_{xy} = 0.351, and ν_{yx} = 0.447. (The x-direction corresponds to the axial direction of the test case and the hoop direction of the FWC.)

APPENDIX B - SHAPE AND CORRECTION FACTORS IN STRESS INTENSITY FACTOR EQUATION FOR SURFACE CRACK [14]

$$F = [M_1 + M_2(\frac{a}{t})^2 + M_3(\frac{a}{t})^4]gf_\phi f_w \tag{9}$$

and

$$f_w = \{\sec [(\frac{\pi c}{W})(\frac{a}{t})^{1/2}]\}^{1/2}$$

For $a/c \leq 1$,

$$Q = 1 + 1.464(\frac{a}{c})^{1.65}$$

$$M_1 = 1.13 - 0.09(\frac{a}{c})$$

$$M_2 = -0.54 + \frac{0.89}{0.2 + \frac{a}{c}}$$

$$M_3 = 0.5 - \frac{1}{0.65 + \frac{a}{c}} + 14(1 - \frac{a}{c})^{24}$$

$$g = 1 + [0.1 + 0.35(\frac{a}{t})^2][1 - \sin \phi]^2$$

$$f_\phi = [(\frac{a}{c})^2 \cos^2\phi + \sin^2\phi]^{1/4}$$

and for $a/c > 1$,

$$Q = 1 + 1.464(\frac{c}{a})^{1.65}$$

$$M_1 = [1 + 0.04(\frac{c}{a})](\frac{c}{a})^{1/2}$$

$$M_2 = 0.2(\frac{c}{a})^4$$

$$M_3 = -0.11(\frac{c}{a})^4$$

$$g = 1 + [0.1 + 0.35(\frac{c}{a})(\frac{a}{t})^2][1 - \sin \phi]^2$$

$$f_\phi = [(\frac{c}{a})^2 \sin^2\phi + \cos^2\phi]^{1/4}$$

REFERENCES

1. Poe, Jr., C. C.; Illg, W.; and Garber, D. P.: A Program to Determine the Effect of Low-velocity Impacts on the Strength of the Filament-wound Rocket Motor Case for the Space Shuttle. NASA TM-87588, September 1985.

2. Poe, Jr., C. C.; Illg, W.; and Garber, D. P.: Tension Strength of a Thick Graphite/epoxy Laminate after Impact by a 1/2-In.-Radius Impacter. NASA TM-87771, July 1986.

3. Poe, Jr., C. C.; Illg, W.; and Garber, D. P.: Strength of a Thick Graphite/epoxy Laminate after Impact by a Blunt Object. NASA TM-89099, February 1987.

4. Poe, Jr., C. C.; and Illg, W.: Tensile Strength of a Thick Graphite/Epoxy Rocket Motor Case After Impact by a Blunt Object. 1987 JANNAF Composite Motor Case Subcommittee Meeting, CPIA Publication 460, Feb. 1987, pp. 179-202.

5. Poe, Jr., C. C.; Illg, W.; and Garber, D. P.: Hidden Impact Damage in Thick Composites. Proceedings of the Review of Progress in Quantitative Nondestructive Evaluation, Vol. 5B, pp. 1215-1225, 1986.

6. Madaras, E. I.; Poe, Jr., C. C.; Illg, W.; and Heyman, J. S.: Estimating Residual Strength in Filament Wound Casings from Non-Destructive Evaluation of Impact Damage. Proceedings of the Review of Progress in Quantitative Nondestructive Evaluation, Vol. 6B, pp. 1221-1230, 1986.

7. Madaras, E. I.; Poe, Jr., C. C.; and Heyman, J. S.: Combining Fracture Mechanics and Ultrasonics NDE to Predict the Strength Remaining in Thick Composites Subjected to Low-Level Impact. 1986 Ultrasonics Symposium Proceedings, Ed. B. R. McAvoy, New York, Institute of Electrical and Electronic Engineers. Vol. 86CH2375-4, No. 2, pp. 1051-1059.

8. Madaras, E. I.; Poe, Jr., C. C.; and Heyman, J. S.: A Nondestructive Technique for Predicting the Strength Remaining in Filament Wound Composites Subjected to Low-Level Impact. 1987 JANNAF Composite Motor Case Subcommittee Meeting, CPIA Publication 460, Feb. 1987, pp. 249-258.

9. Poe, Jr., C. C.: Simulated Impact Damage in a Thick Graphite/epoxy Laminate Using Spherical Indenters. NASA TM-100539, 1988.

10. Greszczuk, Longin B.: Damage in Composite Materials due to Low Velocity Impact. Impact Dynamics, John Wiley & Sons, Inc., 1982, pp. 55-94.

11. Love, A. E. H.: The Stress Produced in a Semi-infinite Solid by Pressure on Part of the Boundary. Phil. Trans. Roy. Soc. Lond. Series A, vol. 228, 1929, pp. 377-420

12. Harris, C. E.; and Morris, D. H.: Preliminary Report on Tests of Tensile Specimens with a Part-Through Surface Notch for a Filament-Wound Graphite/Epoxy Material. NASA CR-172545, 1985.

13. Harris, C. E.; and Morris, D. H.: The Fracture of Thick Graphite/Epoxy Laminates with Part-Through Surface Flaws. Composite Materials: Fatigue and Fracture, ASTM STP 907, American Society for Testing and Materials, 1986, pp. 100-114.

14. Newman, Jr., J. C.; and Raju, I. S.: Stress-Intensity Factor Equations for Cracks in Three-Dimensional Finite Bodies. Fracture Mechanics: Fourteenth Symposium--Volume I: Theory and Analysis, ASTM STP 791, American Society for Testing and Materials, 1983, pp. I-238-I-268.

15. Poe, Jr., C. C.: A Paramteric Study of Fracture Toughness of Fibrous Composite Materials. NASA TM-89100, 1987.

16. Harris, C. E.; and Morris, D. H.: Fracture Behavior of Thick, Laminated Graphite/Epoxy Composites. NASA CR-3784, 1984.

17. Wu, Bing-Hua; and Erdogan, F.: The surface Crack Problem in an Orthotropic Plate Under Bending and Tension. NASA CR-178281, April, 1987.

18. Chatterjee, S. N.: Surface Cracks in Thick Laminated Composite Plates. Presented at the ASTM/SEM Symposium on Surface Crack Growth: Models, Experiments and Structures, April 25, 1988, Reno, Nevada.

Table I. Properties of constituents of composite.

	Helical fiber	Broadgoods fiber	Matrix
Tensile modulus, GPa (Msi) ...	228 (33)	228 (33)	2.85 (0.414)
Poisson's ratio	-	-	.35
Tensile strength, GPa (ksi) ..	3.96 (574)	.75 (544)	-
Elongation at failure	0.0167	-	-
Density, kg/m^3 ($lbm/in.^3$)	1790 (0.0648)	1780 (0.0642)	1230

Table II. Physical properties of composite.

Composite density, kg/m^3 ($lbm/in.^3$) ..	1490 (0.05397)
Resin mass fraction	0.3459
Resin volume fraction	0.3845
Fiber volume fraction	0.5449
Void content	0.07062

Table III. Composite lamina properties

	Unidirectional broadgoods	Helical layers	Cut helical layers	Cloth
E_{11}, GPa (Msi)	1.06 (15.4)	111 (16.2)	111 (16.2)	59.3 (8.60)
E_{22}, GPa (Msi)	6.39 (0.927)	1.92 (0.278)	1.92 (0.278)	59.3 (8.60)
G_{12}, GPa (Msi)	4.47 (0.649)	4.28 (0.621)	4.28 (0.533)	3.68 (0.533)
ν_{12}	0.275	0.267	0.267	0.0348
Thickness per layer, mm (in.)	[a]0.427 (0.0168)	0.427 (0.0168)	0.711 (0.0280)	0.427 (0.0168)

[a]Equal to three plies of broadgoods.

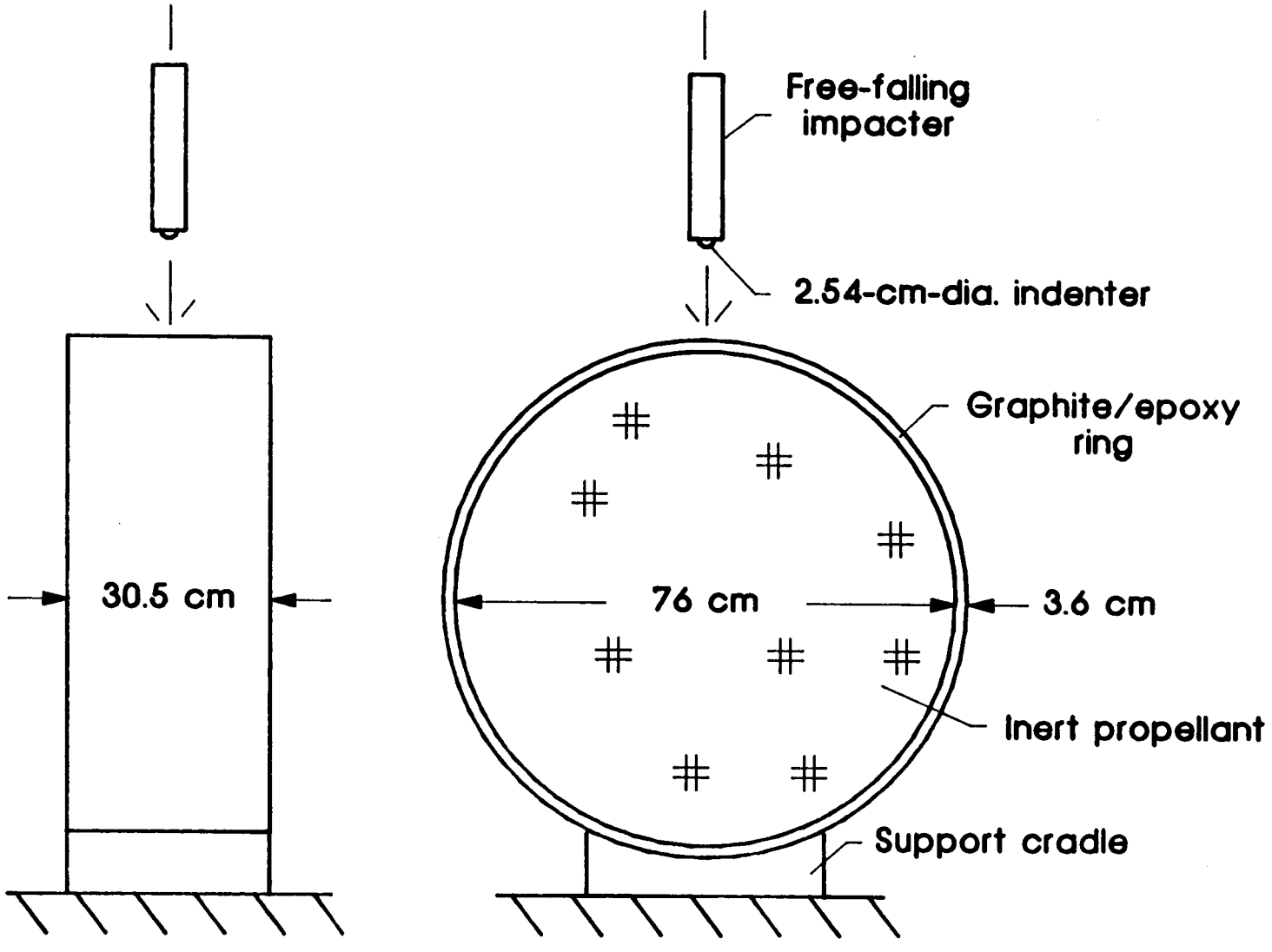

Figure 1.- Impact tests of FWC-like ring.

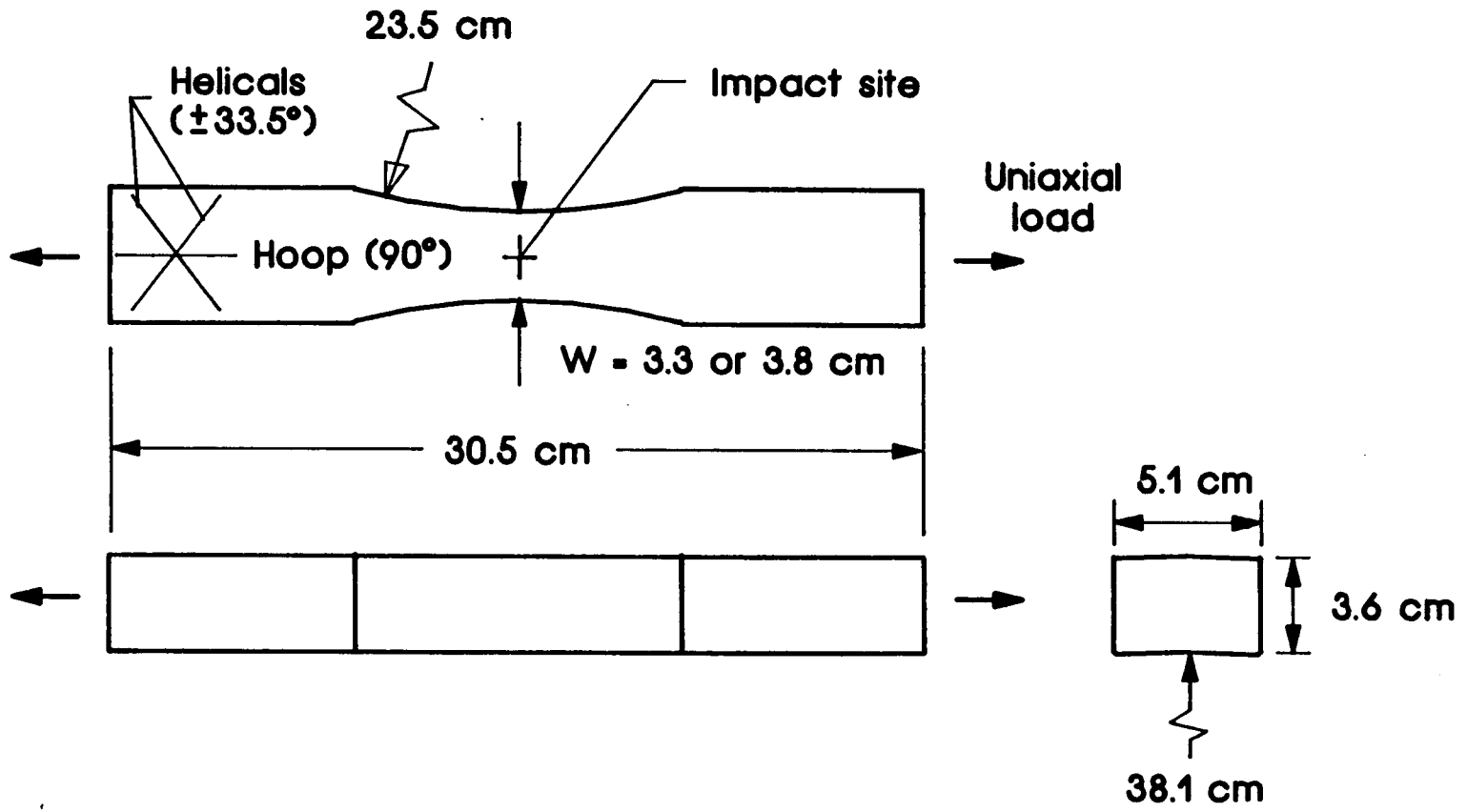

Figure 2.- Sketch of tensile specimen with impact damage.

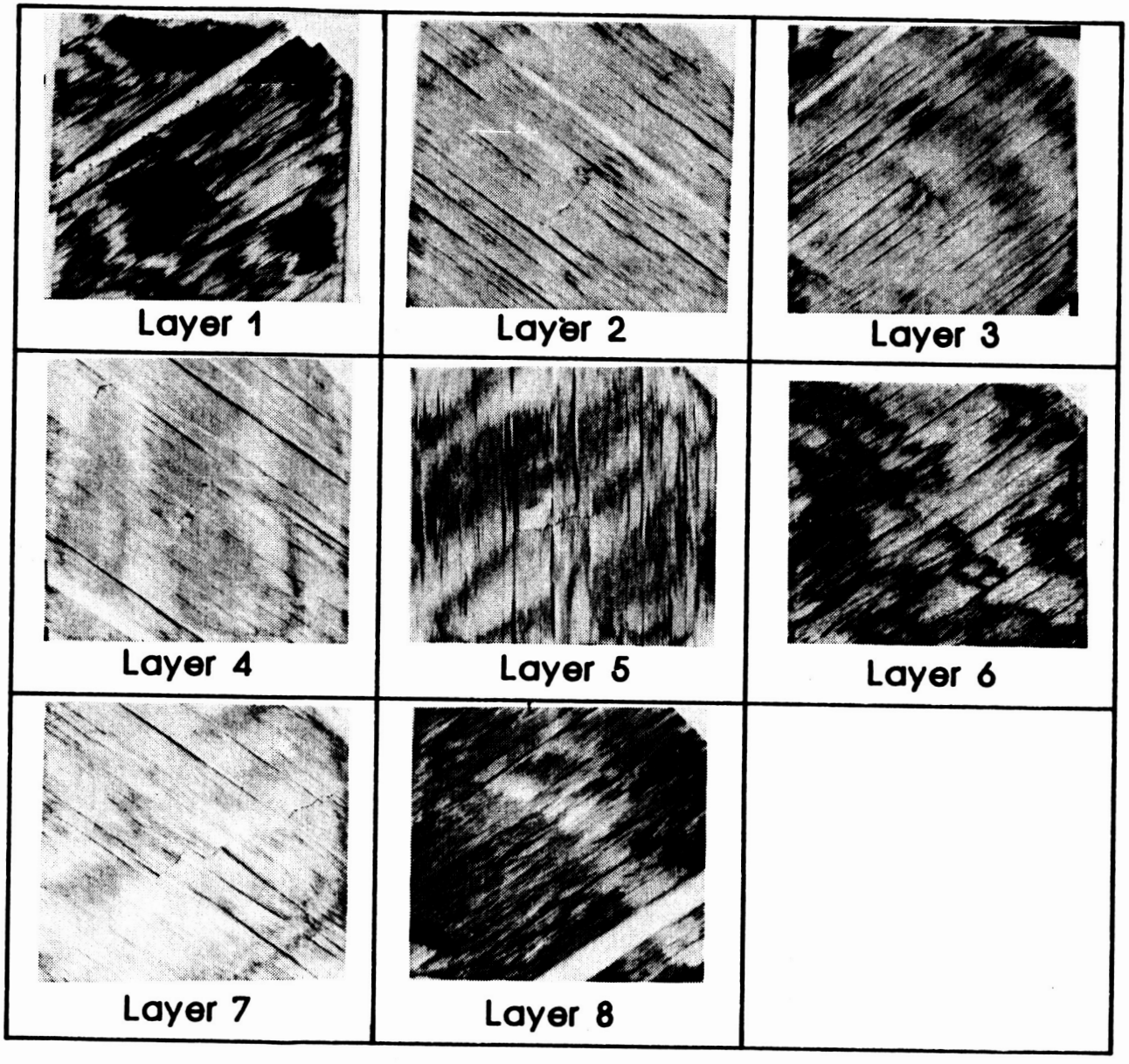

Figure 3.- Fiber damage caused by simulated impact force of 66.7 kN with 2.54-cm-dia. indenter.

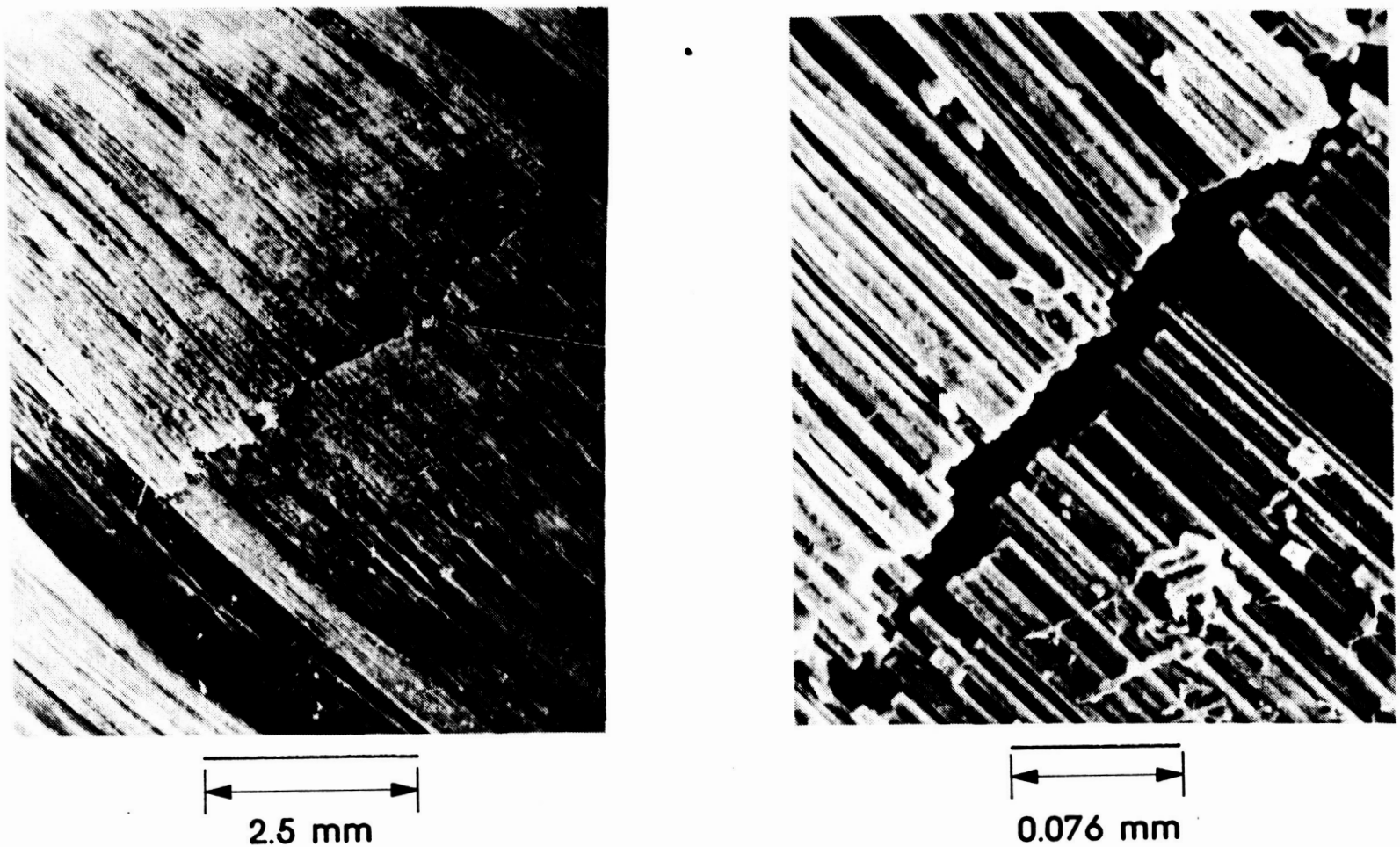

Figure 4.- Photomicrographs of fiber damage in layer 7 (the deepest with damage) caused by impact force of 54.3 kN with 2.54-cm-dia. indenter.

FIG4.AST

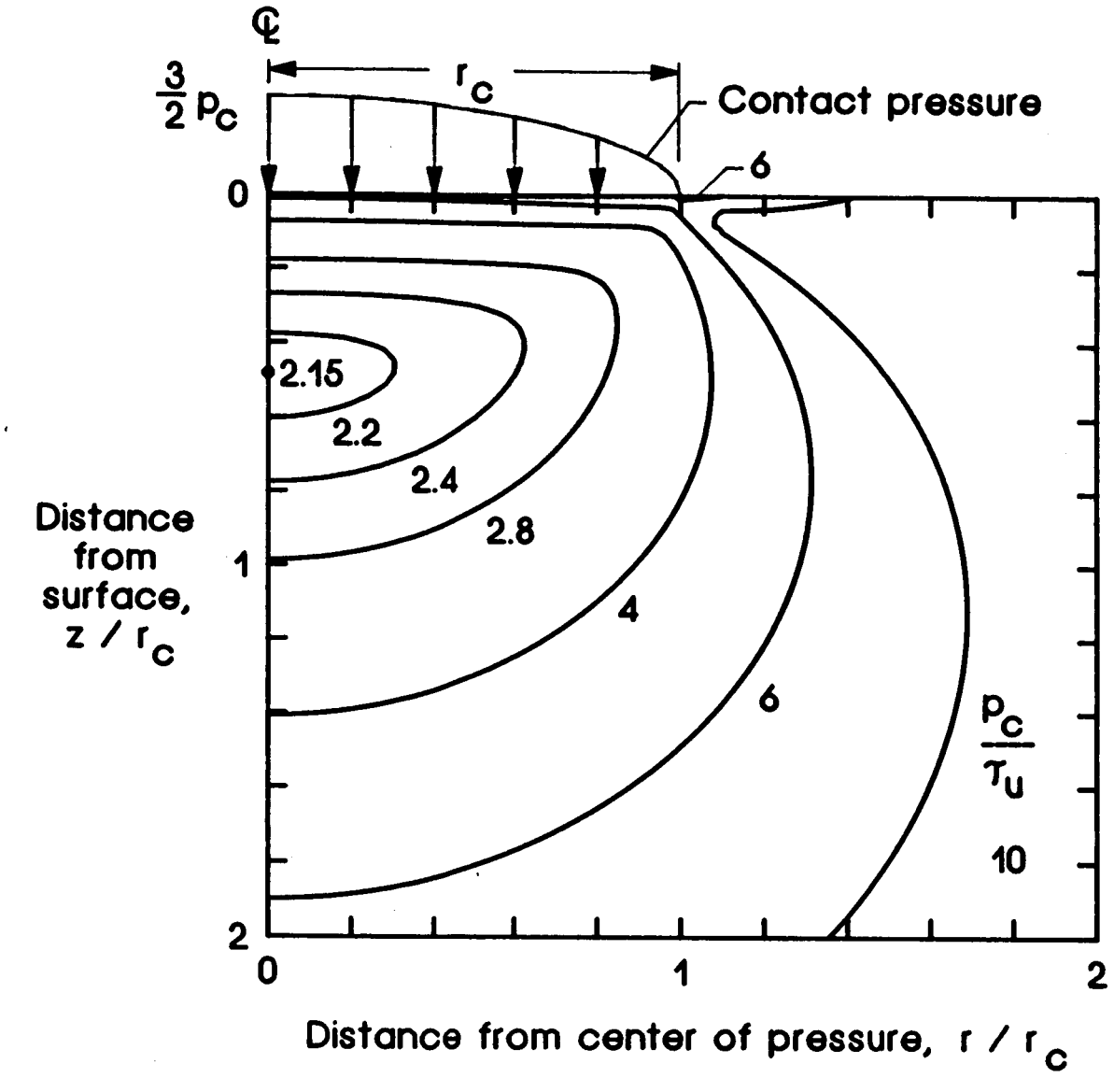

Figure 5.- Damage contours according to Love's solution (Poisson's ratio = 0.3).

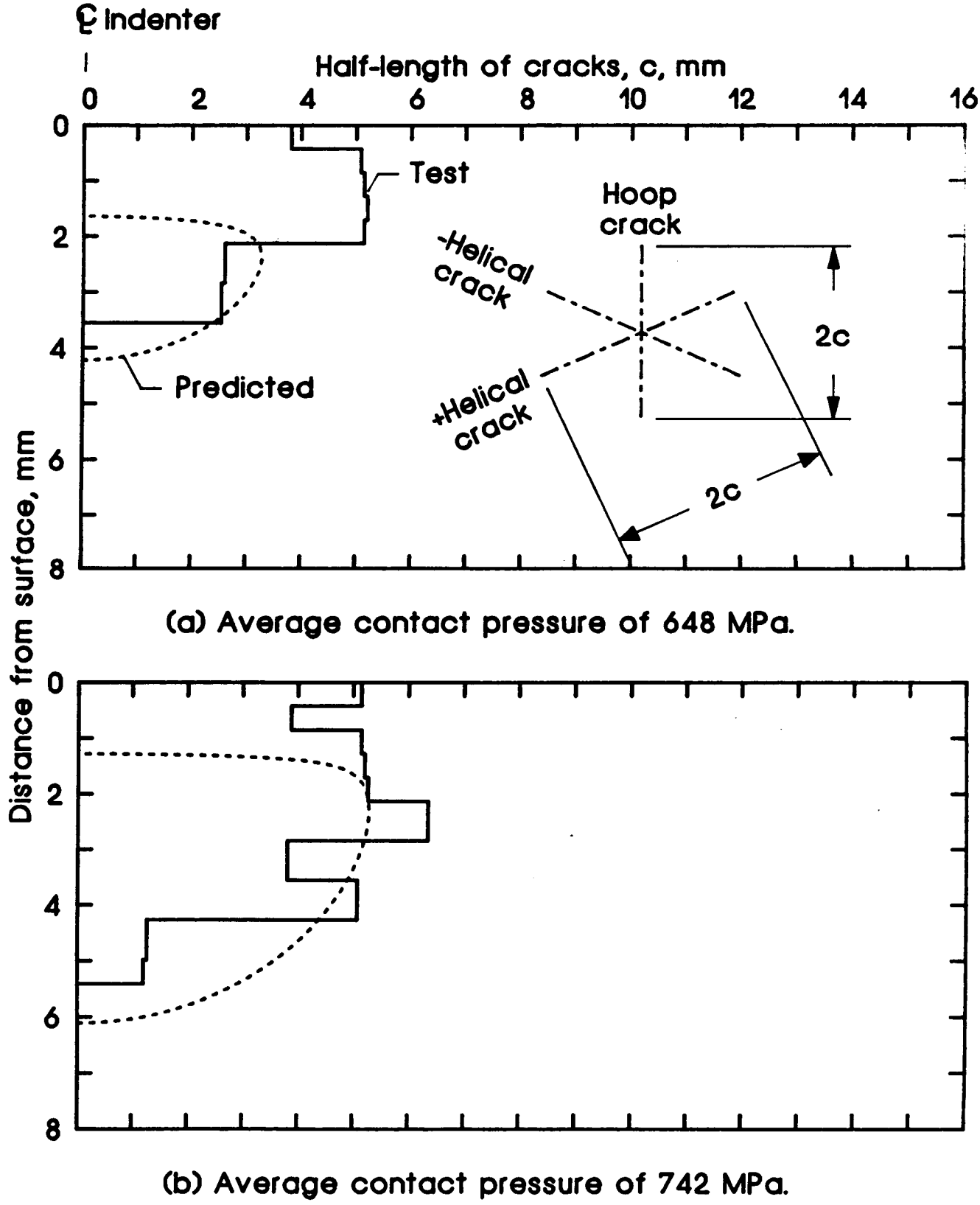

Figure 6.- Comparison of measured and predicted (T_u = 276 MPa) damage profiles.

FIG6.AST

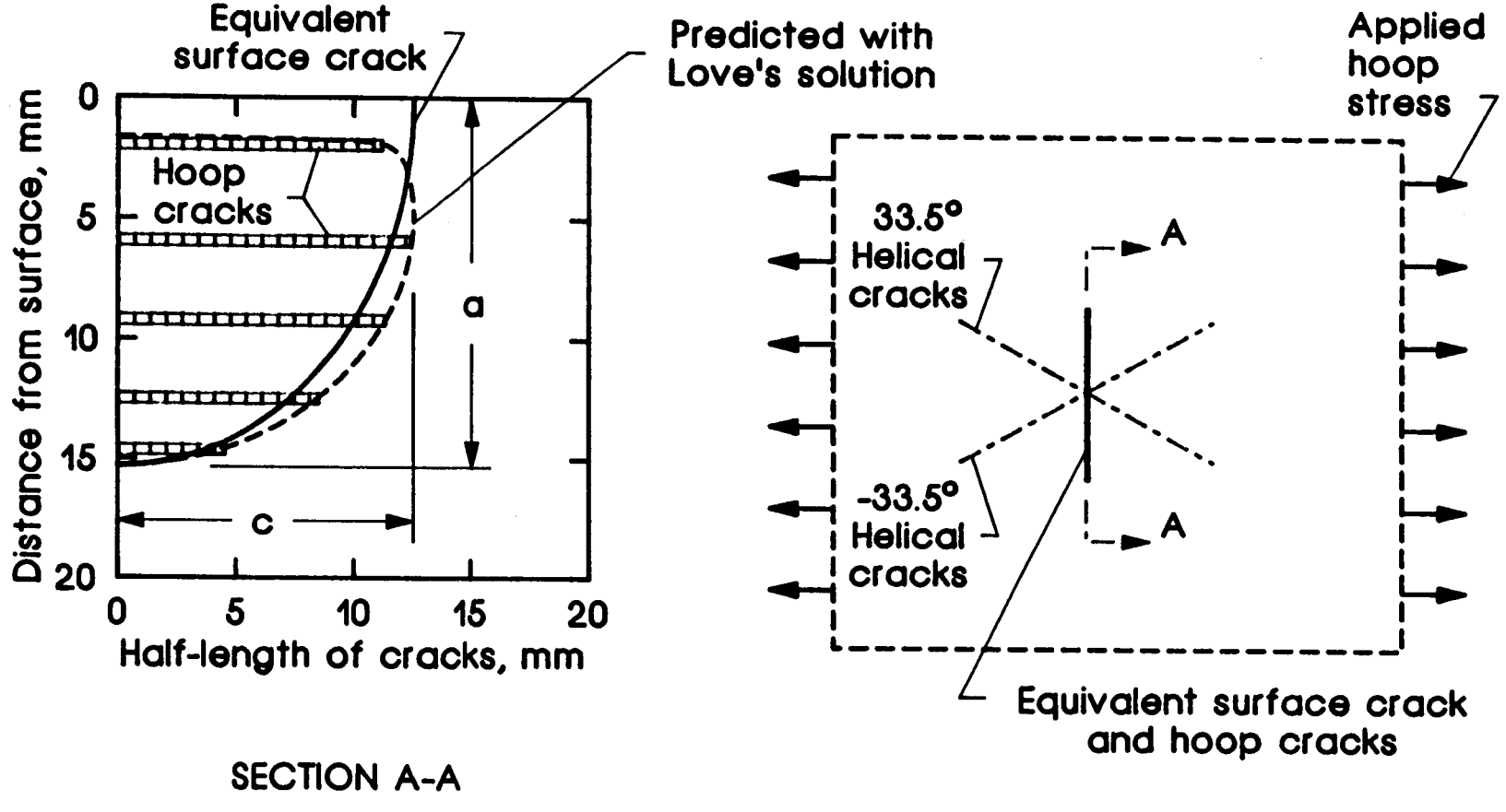

Figure 7.- Equivalent surface crack for impact damage.

FIG7.AST

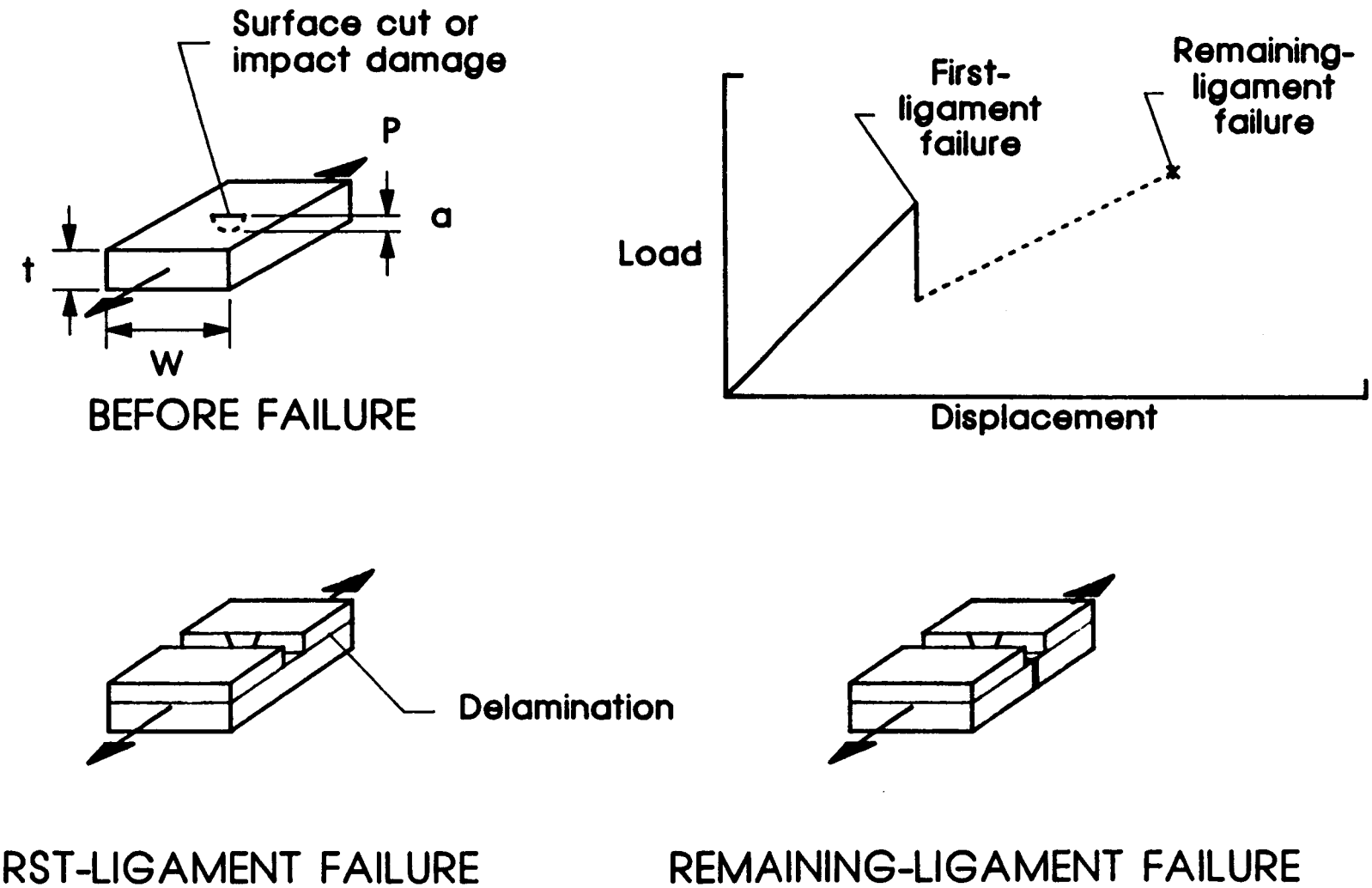

Figure 8.- Two-part failure with surface cut or impact damage.

FIG8.AST

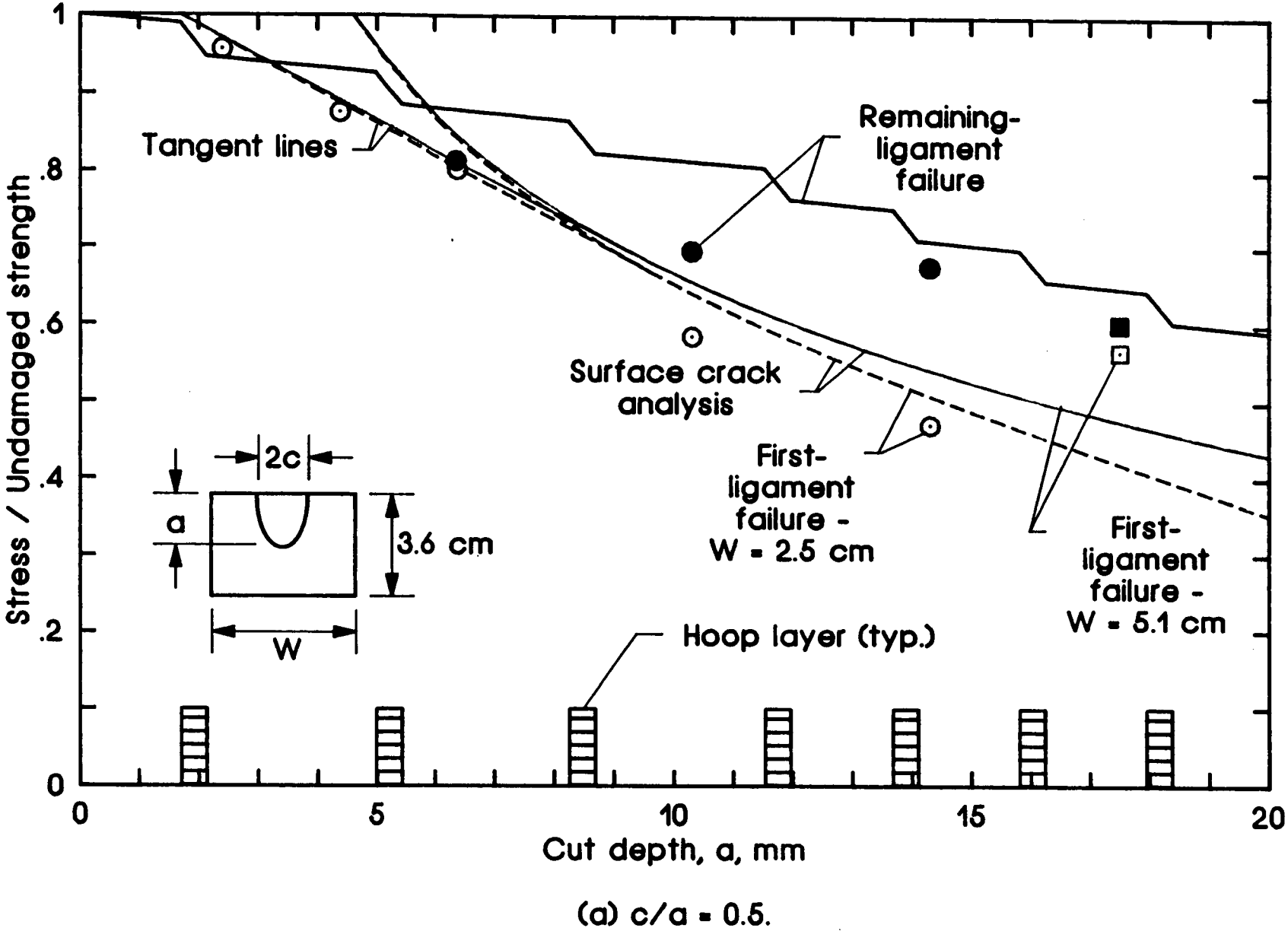

(a) c/a = 0.5.

Figure 9.- Average strengths for FWC laminate with surface cuts.

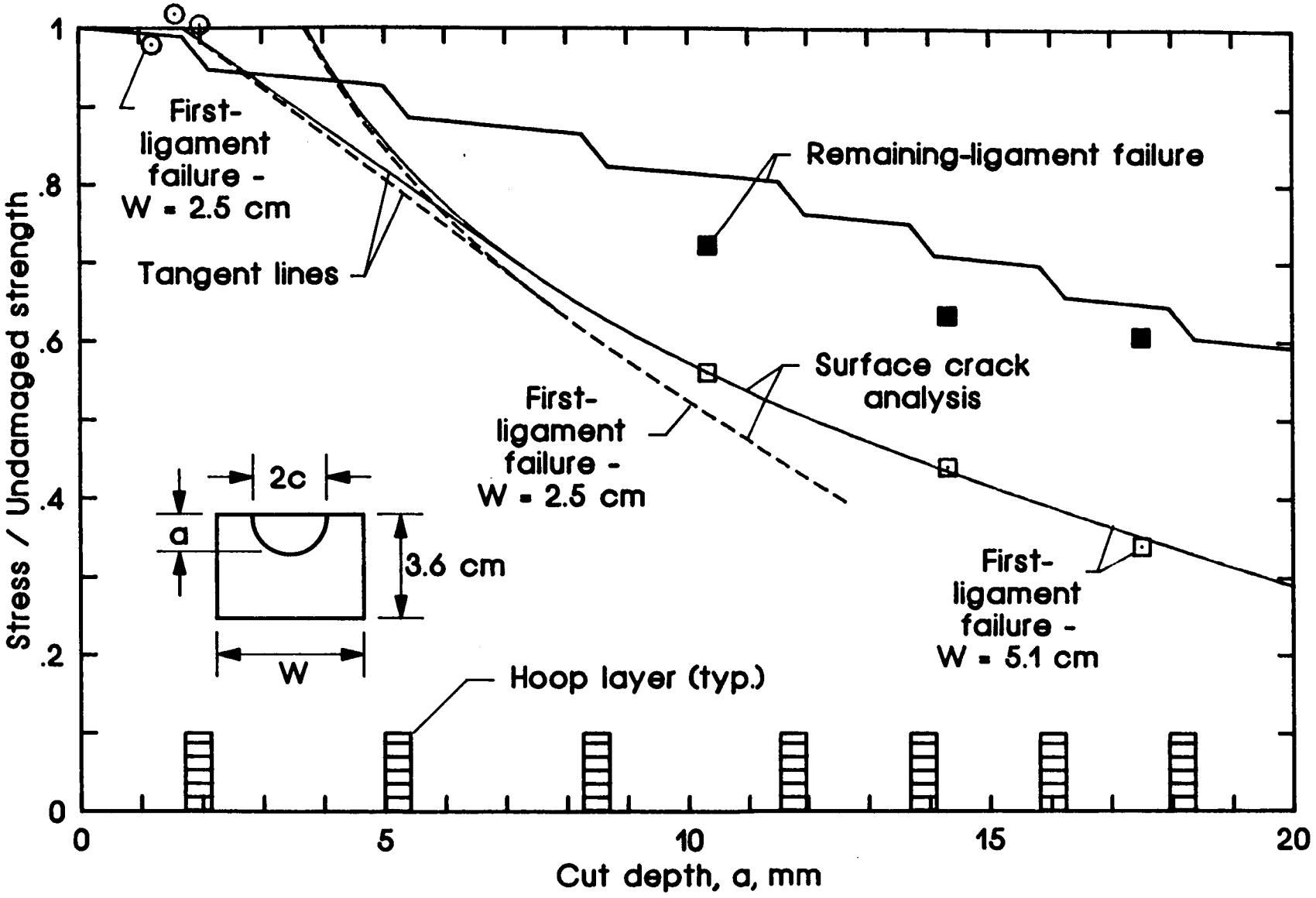

(b) c/a = 1.0.

Figure 9.- Continued.

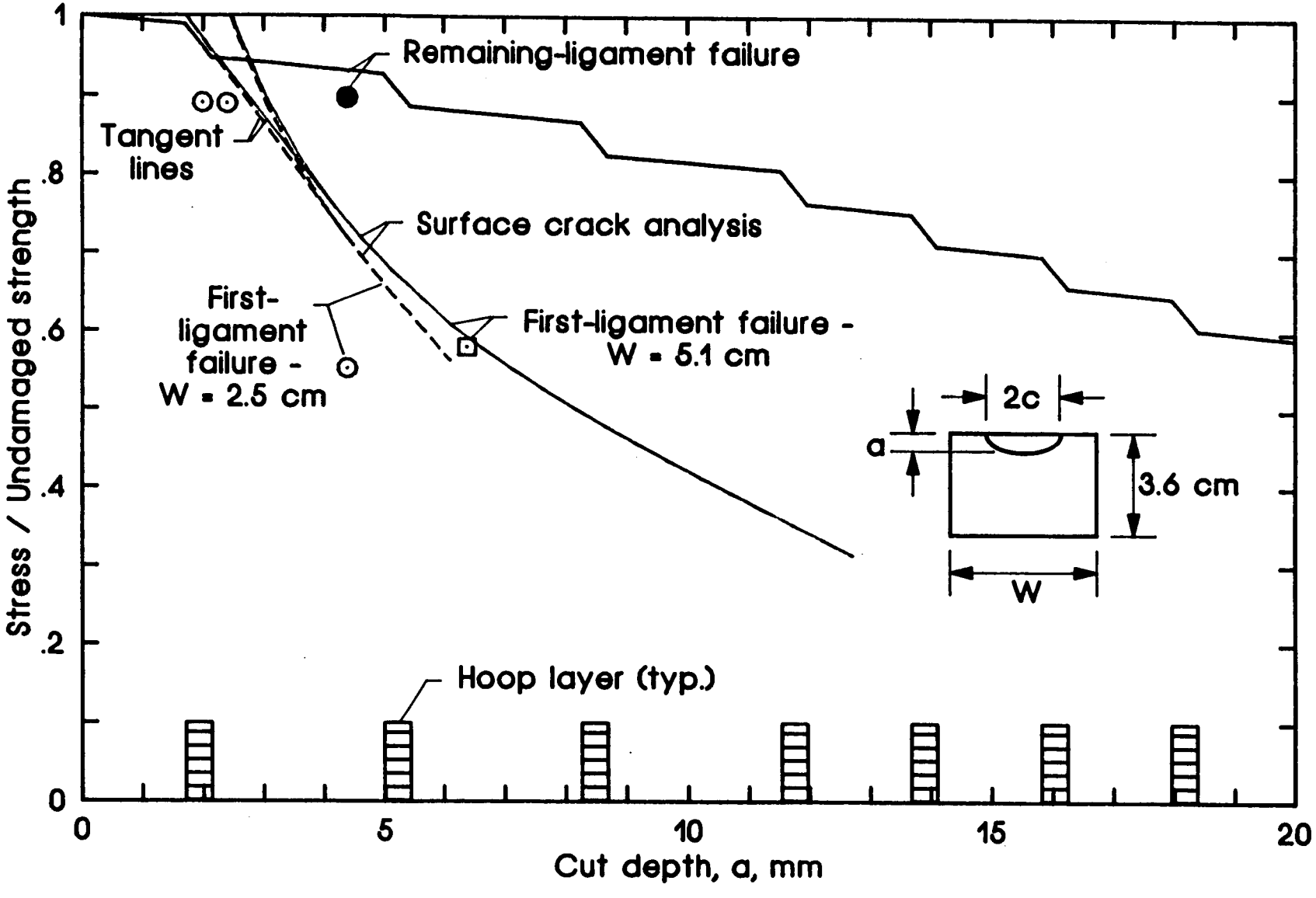

(c) c/a = 2.0.

Figure 9.- Continued.

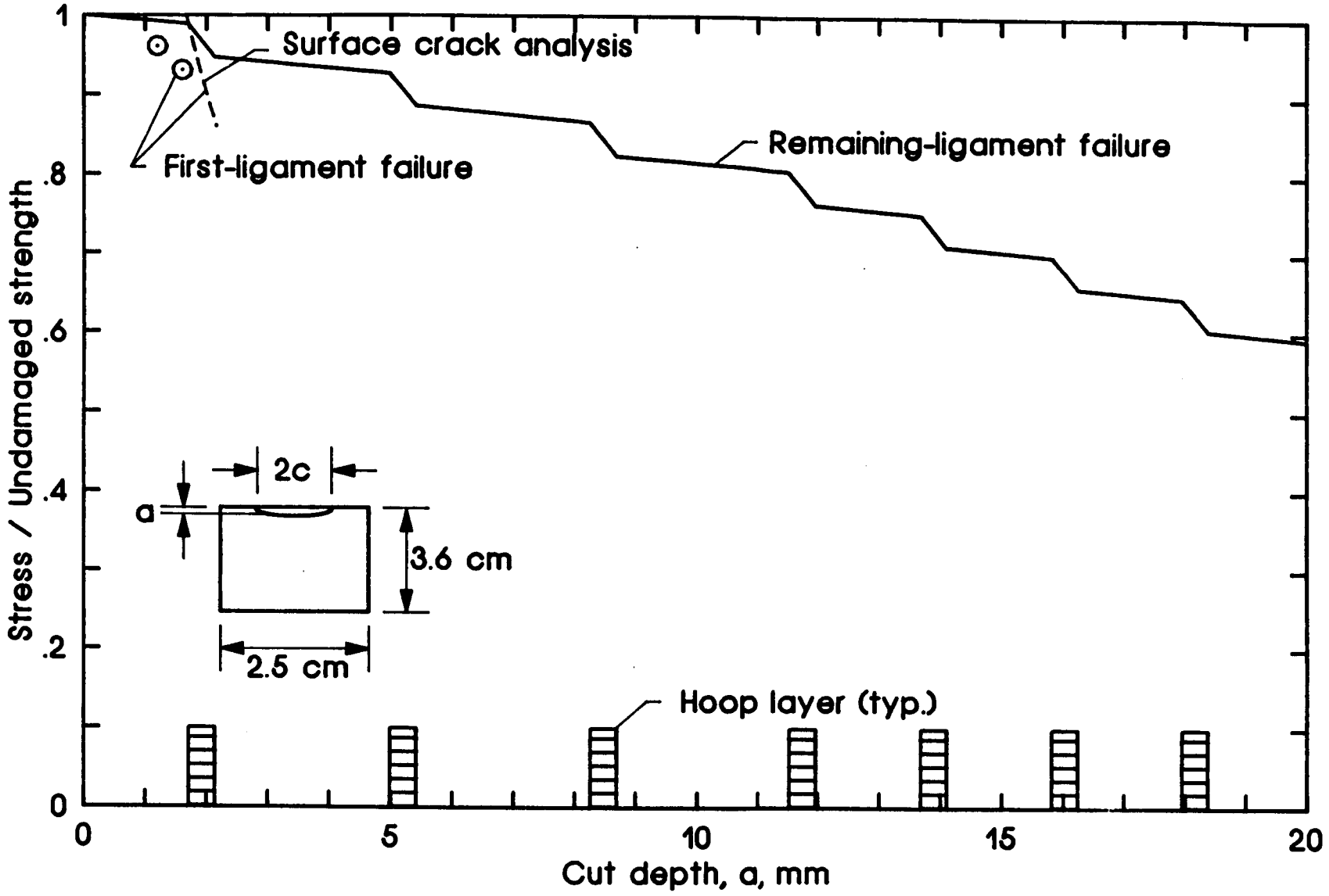

(d) c/a = 5.7.

Figure 9.- Concluded.

FIG9D.AST

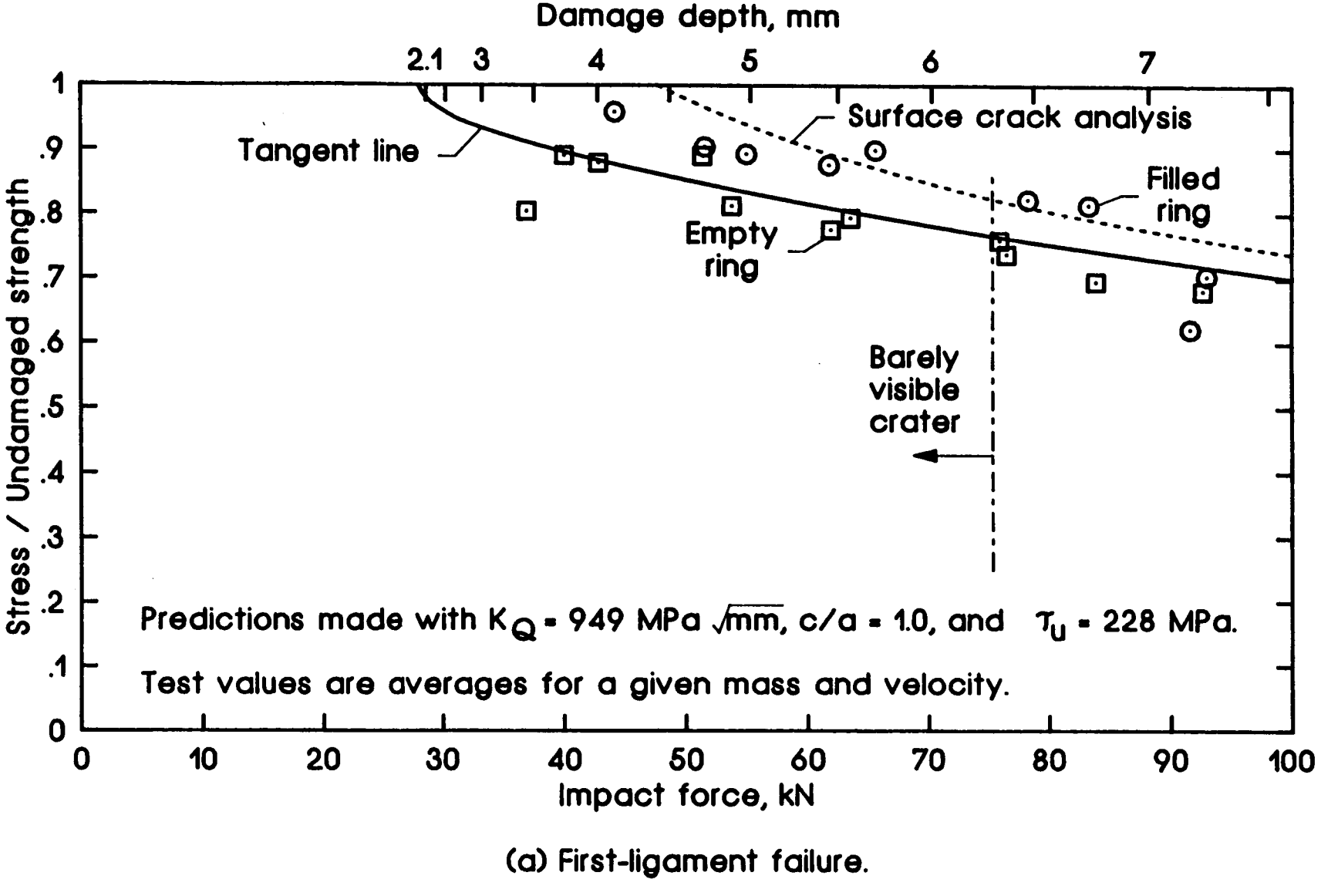

(a) First-ligament failure.

Figure 10.- Measured and predicted strengths for FWC laminate with impact damage.

FIG10A.AST

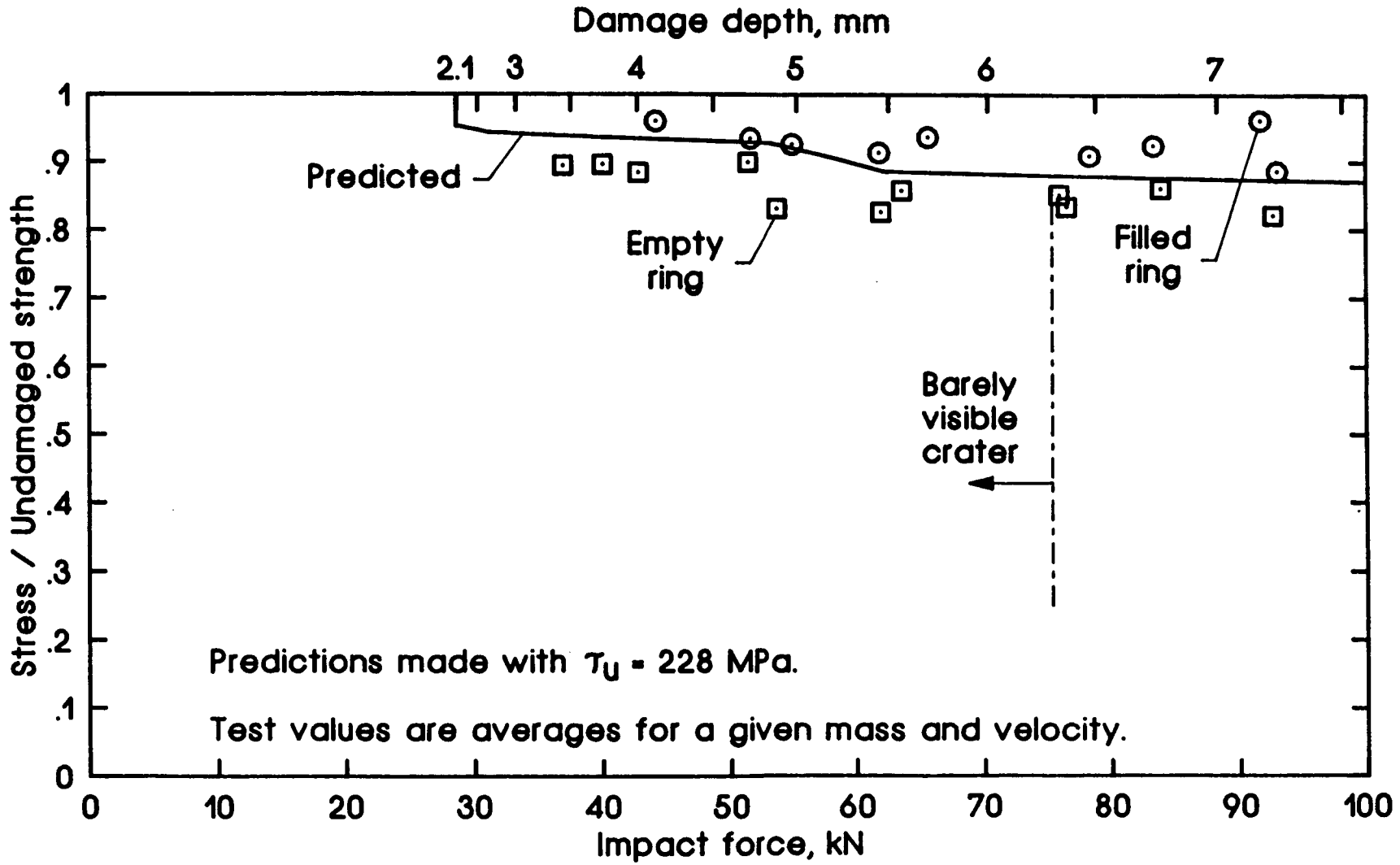

(b) Remaining-ligament failure.

Figure 10.- Concluded.

FIG10B.AST

1. Report No.	2. Government Accession No.	3. Recipient's Catalog No.
NASA TM-100600		

4. Title and Subtitle	5. Report Date
Surface Crack Analysis Applied to Impact Damage In a Thick Graphite/Epoxy Composite	April 1988
	6. Performing Organization Code
7. Author(s)	8. Performing Organization Report No.
C. C. Poe, Jr., C. E. Harris, and D. H. Morris	
	10. Work Unit No.
9. Performing Organization Name and Address	506-43-11-04
Natioanl Aeronautics and Space Administration Langley Research Center Hampton, Virginia 23665-5225	11. Contract or Grant No.
	13. Type of Report and Period Covered
12. Sponsoring Agency Name and Address	Technical Memorandum
National Aeronautics and Space Administration Washington, DC 20546-0001	14. Army Project No.

15. Supplementary Notes

C. C. Poe, Jr., and C. E. Harris, Langley Research Center, Hampton, VA
D. H. Morris, Virginia Polytechnic Institute and State University, Blacksburg, VA

16. Abstract

The residual tensile strength of a thick graphite/epoxy composite with impact damage was predicted using surface crack analysis. The damage was localized to a region directly beneath the impact site and extended only part way through the laminate. The damaged region contained broken fibers, and the locus of breaks in each layer resembled a crack perpendicular to the direction of the fibers. In some cases, the impacts broke fibers without making a visible crater. The impact damage was represented as a semi-elliptical surface crack with length and depth equal to that of the impact damage. The maximum length and depth of the damage were predicted with a stress analysis and a maximum shear stress criterion. The predictions and measurements of strength were in good agreement.

17. Key Words (Suggested by Author(s))	18. Distribution Statement
Graphite/epoxy Composite Filament winding Motor case Impact damage Fracture Surface crack	Unclassified - Unlimited Subject Category 24

19. Security Classif. (of this report)	20. Security Classif. (of this page)	21. No. of Pages	22. Price*
Unclassified	Unclassified	31	A03

*For sale by the National Technical Information Service, Springfield, Virginia 22161